Measurement Based Modelling of In-Train Repeater Deployments

Martin Lerch*, Philipp Svoboda*, Daniel Maierhofer*, Josef Resch†,
Alexander Brantner†, Vaclav Raida*, and Markus Rupp*
*Institute of Telecommunications, TU Wien, Austria
†ÖBB Technische Services GmbH, Austria
mlerch@nt.tuwien.ac.at

***Abstract*—In recent years, the demand of train-commuting nomadic users for the Internet has been a huge challenge for train and mobile operators. Consequently, train operators have started to deploy in-train repeater systems to increase mobile users' service quality. These systems generally follow the structure of static deployments. However, in contrast to a static deployment where the system is set up once using constant parameters that are based on an initial measurement, the train will commute in dense urban city centers and sparsely populated rural areas. We propose a holistic model that helps to understand the role of each system component, namely, cabin pathloss, repeater model, window penetration loss, and outdoor pathloss, in which each individual element can be measured independently. We parametrize the model by measuring an existing in-train repeater deployment of a high-speed train. Finally, we have analyzed the operation of the complete system for two extreme cases of deployment strategy: simple rural and optimized track side. We show that the main benefit of the tested system is visible in the nonoptimized rural deployment. However, the optimized deployment also benefits from the repeater setup.**

I. Introduction

The ubiquity of the internet is one of the major drivers of the digital transformation. Nomadic users who access cloud services rely on the omnipresent digital link to the Internet, which is typically offered by mobile wireless networks that provide a seamless connection. The performance of radio networks is closely linked to the density of base stations via the experienced pathloss, especially in rural areas, where a low density results in low performance and limited access. Moreover, the additional penetration loss from walls and windows of a building makes it difficult to provide indoor users with high-rate services from a rural-coverage network level. Thus, a generic solution to this challenge would be to use static repeater systems that pick up the signal from outside the building, amplify the signal, and then use a distribution system to deploy the signal inside the building. These systems, called amplify-and-forward systems, can minimize the impact of the additional pathloss due to walls and other parts of the building. In recent years, the above-mentioned issue has posed a similar challenge to mobile networks due to the demand of train-commuting nomadic users for internet access. Due to the metal structure of the railroad cabin, majority of the radio signal is received through the windows. The metalized coating of windows is installed for better thermal isolation; however, this adds to pathloss in a railroad cabin, which makes it difficult for internet users to access high-rate services while traversing the rural areas on an inter-city rail connection on board of an express passenger train. Consequently, railroad operators have recently started to deploy repeater systems in train cabins. These systems generally follow the structure for static deployments. However, in contrast with a static deployment, in which the system is set up once using constant parameters that are based on an initial measurement, the train will commute in dense urban city centers and sparsely populated rural areas. Both scenarios are significantly different regarding mobile communication and coverage; a generic static configuration of the system setup cannot cover those elements all at once.

Related Work

Currently, there is extensive literature that discusses the aspects of static repeater deployments for mobile cellular systems (see [1], [2]). These studies focus on extending the coverage for indoor users using amplify-and-forward systems. Channel models for different vehicular scenarios have been extensively researched in the past decade. On the subject of channel models, several researchers have analyzed and measured the radio channel parameters of antennas on train rooftops (see [3]–[6]). In particular, the papers have covered channel measurements, analysis, and models for communication systems connecting to high-speed trains. However, current state-of-the art simulation environments still lack realistic models of train cabins (see [7], [8]). Experimental studies are analyzing the service improvement of a repeater deployment by drawing measurement samples along a track (see [9]–[11]). These studies have analyzed the in-train coverage of mobile cellular users based on samples collected from an operational LTE network with an existing repeater deployment. However, optimization based on this approach requires an time consuming iterration over all parameters. To our knowledge, there is no literature on modeling repeater deployments in vehicular scenarios that allows for direct optimization.

Our Contribution

We propose a holistic model for an in-train repeater (ITR) deployment derived from measurements of an existing ITR setup. The model is built from blocks, where each can be parametrized independently, by measurement or by prior knowledge.

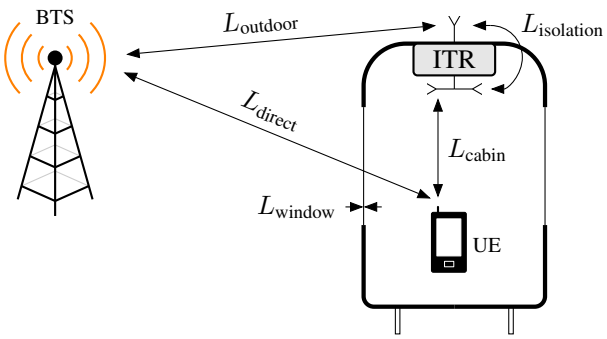

Fig. 1. Holistic in-train repeater model.

II. Model

Our system consists of a base-station (BTS) and a user equipment (UE) on board a train equipped with an ITR. We model the link between the BTS and the UE as a two-path pathloss model. Figure 1 illustrates the system and all the parameters considered in the model. Here, L_{direct} describes the direct path between the BTS and the UE onboard the train, and corresponds to the case where no ITR is used. The second path is the path through the repeater. Its pathloss is given by $L_{\text{repeater}} = L_{\text{outdoor}} - G + L_{\text{cabin}}$, where G is the gain of the ITR. The total pathloss experienced by the UE is given in the linear domain by

$$L_{\text{UE}} = \frac{L_{\text{direct}} \cdot L_{\text{repeater}}}{L_{\text{direct}} + L_{\text{repeater}}}. \tag{1}$$

Furthermore, we consider the isolation of the train carriage through $L_{\text{isolation}}$, and L_{window} describes the penetration loss of the windows.

A. Parameters

To parametrize our model, we distinguish between the environment-specific parameters and the parameters that depend on the train and the ITR only. The parameters that are independent of the environment can be measured in any environment, whereas drive-tests are necessary to measure the environment-specific parameters. The environment-specific parameters are as follows:

- The outdoor pathloss L_{outdoor} is the pathloss from the BTS to the pick-up antenna on the rooftop of the train that is connected to the ITR. For a given setup, L_{outdoor} can be measured in a single drive-test along the railroad track of interest. In Section VI, we present the results for two specific railroad tracks.
- L_{direct} is the pathloss of the direct path between the BTS and the UE on board the train. Compared to the outdoor pathloss L_{outdoor}, this pathloss depends on the train under test and the location of the UE inside the train. Thus, many drive-tests are necessary to measure the direct pathloss for a specific train along a specific railroad track. Hence, we consider defining a lower bound rather than measuring it (see Section VII).
- The pathloss $L_{\text{isolation}}$ between the antenna inside the train and that on the train rooftop describes the isolation of the train. The actual value of the isolation depends on the train carriage, the antennas used, and the presence of reflecting objects in the vicinity of the train. In our setup, for frequencies of 800 MHz…2600 MHz, the isolation is larger than 80 dB when measured inside a train workshop.

The parameters that are independent of the environment are as follows:

- The pathloss L_{cabin} between the indoor port of the repeater and the UE depends on the indoor antenna, the antenna of the UE, and the location of the UE inside the train. Assuming a sufficient high-penetration loss of the train, L_{cabin} is independent of the environment. See Section III for the measurement results of our specific setup.
- We define the penetration loss L_{window} of the train windows as an additional loss when the windows are inserted into an existing path. See Section IV for the measurement results of the windows of our specific train.
- The gain G of the ITR depends on the repeater considered and the actual receive power. It is upper bounded by the isolation of the train. As a rule of thumb [12], the gain G of the repeater should be at least 15 dB lower than the isolation $L_{\text{isolation}}$ of the train in order to avoid feedback loops. In Section V, we provide a repeater model based on a commercial amplify-and-forward repeater.

Note that aside from the penetration loss of the windows, all pathlosses defined in our model describe the loss of power between two antenna ports. Furthermore, note that all the parameters considered are generally frequency-dependent.

III. The Cabin Pathloss

We assume that the propagation conditions inside the vehicle are independent of the environment of the vehicle. Therefore, the measurements of the penetration loss of the train windows under test have shown that the penetration loss is at least 11 dB (see [13]). Thus, possible reflections of objects located outside the train are negligible, and the measured cabin pathloss is independent of the environment.

A. Setup under Test

The test setup is deployed on board a high-speed train, namely, railjet, operated by the National Austrian Railway company ÖBB. Figure 2 shows the train being tested. It is equipped with an ITR system that uses radiating cables to supply the users on board the train. One ITR supplies four train carriages whereas the ITR is located approximately in the middle of these four carriages where the output power of the ITR is equally split among the two pairs of carriages.

B. Measurement Methodology

To measure the cabin pathloss, we replace the ITR with a signal generator that continuously transmits the same 20 MHz LTE-like OFDM signal. We measure the received power using

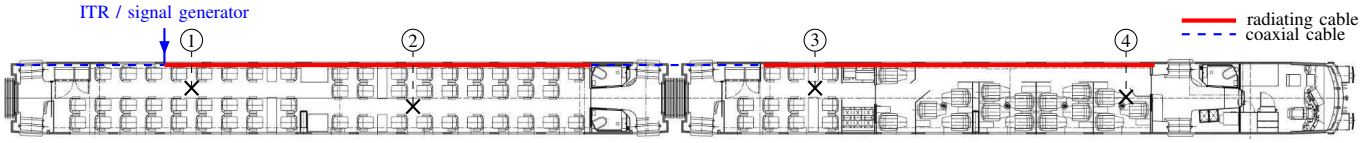

Fig. 2. Setup of the repeater deployment in an Austrian railjet.

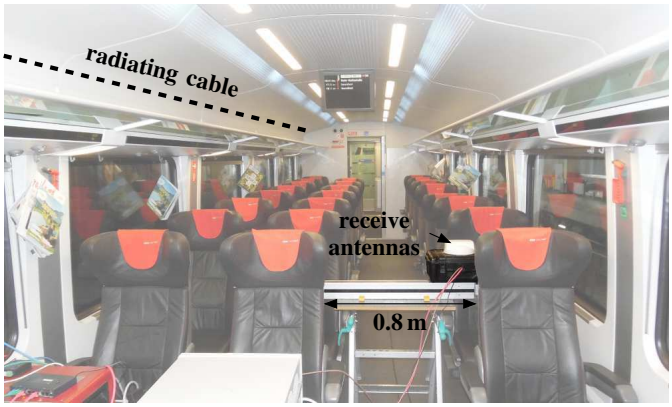

Fig. 3. Measurement setup to measure the cabin pathloss. The picture shows measurement location 2.

TABLE I
MEASUREMENT PARAMETERS

Center frequencies f_c	842 MHz, 895 MHz, 1745 MHz, 1940 MHz, 2510 MHz
Transmit antenna	radiating cable
Signal source	Rohde & Schwarz SMU 200A
Transmit signal	OFDM, 1200 subcarriers @ Δf=15 kHz
Receive antenna	Panorama antennas' "Great White" [15]
Receiver	Keysight N9020A

the setup shown in Figure 3. Similar to [14] we combat small-scale fading by using a linear guide to measure the received power at 20 different positions within a length of 0.8 m. Furthermore, we measure the received power at two different polarizations of the receive antenna. The results are then averaged over all positions and polarizations. We then repeat the measurement in five bands from 800 MHz. . . 2600 MHz to capture the frequency-dependence. We performed the measurements in the corresponding uplink (UL) bands to avoid measuring interference. The whole procedure is then performed at four different locations marked in Figure 2. Table I details all the measurement parameters.

C. Measurement Results

The measurement results for all frequency bands and all measurement locations are shown in Table II. As common for a radiating cable, the pathloss at different locations, for one frequency, shows only a small variation within the same cabin. In general, the loss increases as frequency increases. The step in pathloss from location 2 to 3 originates from the coupling between the cabins, which increases with frequency. The minimum pathloss can be found in location 2, close to

TABLE II
CABIN PATHLOSS

f_c	①	②	③	④
842 MHz	58.4 dB	53.8 dB	60.8 dB	62.4 dB
895 MHz	57.5 dB	54.9 dB	59.9 dB	62.1 dB
1745 MHz	58.7 dB	55.5 dB	66.9 dB	64.9 dB
1940 MHz	58.3 dB	54.1 dB	66.7 dB	65.5 dB
2510 MHz	58.6 dB	58.4 dB	72.6 dB	70.1 dB

the middle of the radiating cable. Overall, the difference in pathloss, for one frequency and in all locations, is below 12 dB. In the setup being tested, one ITR serves two sets of cabins via a power splitter. Therefore, the UL pathloss is approximately 3 dB smaller than the downlink (DL) pathloss measured.

IV. WINDOW PENETRATION LOSS

In a previous measurement campaign, we measured the penetration loss of two different kinds of train windows at frequencies 800 MHz. . . 2600 MHz and at azimuthal angles of arrival of 0°. . . 60°. Thereby, we defined the penetration loss of a window as the additional pathloss observed when inserting the window into a line-of-sight path. See [13] for a description of the measurement methodology. The results for the windows used in our train under test are shown in Table III. Thereby, an angle of 0° corresponds to perpendicular penetration of the window.

TABLE III
WINDOW PENETRATION LOSS

	0°	15°	30°	45°	60°
800 MHz	18.1 dB	20.3 dB	19.3 dB	21.0 dB	18.9 dB
1800 MHz	15.1 dB	12.9 dB	13.3 dB	17.2 dB	11.3 dB
2100 MHz	16.5 dB	14.8 dB	16.6 dB	14.5 dB	17.9 dB
2600 MHz	15.9 dB	14.9 dB	15.6 dB	17.2 dB	18.2 d

V. REPEATER MODEL

Our ITR model is based on a commercial multiband repeater [16] that implements a digital amplify-and-forward repeater. Figure 4 illustrates our model of the ITR for one frequency band. It consists of two separate paths: one for the DL and one for the UL. A nominal gain $G_{\mathrm{X},0}$, a maximum output power $P_{\mathrm{X,out,max}}$, and additive noise $P_{\mathrm{n,X}}$ describe each path.

A. Gain Control

For each of the two paths, the actual gain

$$G_{\mathrm{X}} = \min(G_{\mathrm{X},0}, P_{\mathrm{X,out,max}} - P_{\mathrm{X,in}}) \quad (2)$$

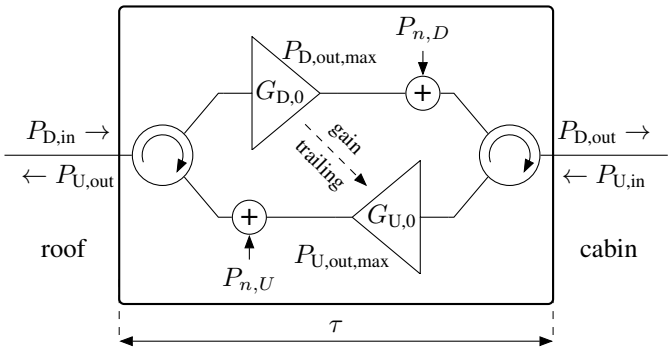

Fig. 4. Block diagram of the in-train repeater.

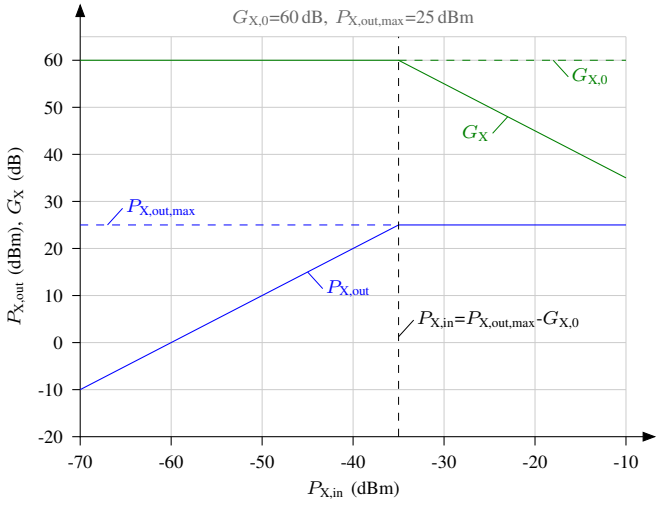

Fig. 5. Relation of input power and available repeater gain.

and the actual output power

$$P_{\mathrm{X,out}} = \min(P_{\mathrm{X,out,max}}, P_{\mathrm{X,in}} + G_{\mathrm{X,0}}) \tag{3}$$

depend on the actual input power $P_{\mathrm{X,in}}$ of the path. For input powers that do not saturate the amplifier ($P_{\mathrm{X,in}} + G_{\mathrm{X,0}} \leq P_{\mathrm{X,out,max}}$), the repeater operates in the linear region. The actual gain G_{X} is equal to the nominal gain $G_{\mathrm{X,0}}$. Otherwise, for $P_{\mathrm{X,in}} + G_{\mathrm{X,0}} > P_{\mathrm{X,out,max}}$, the gain G_{X} decreases such that $P_{\mathrm{X,out}} = P_{\mathrm{X,out,max}}$. Figure 5 illustrates the gain control. To maintain the symmetry of the DL and the UL paths, the UL gain G_{U} may be coupled with the DL gain G_{D} by implementing *gain trailing*. The UL gain can then be described by

$$G_{\mathrm{U}} = \min(G_{\mathrm{D}}, P_{\mathrm{U,out,max}} - P_{\mathrm{U,in}}). \tag{4}$$

B. Noise

We model the transmitted noise $P_{\mathrm{n,X}}$ of the repeater as an additive noise at the output of the repeater to keep the model as general as possible. Doing this would allow the noise power measured at the output of a repeater to be directly applied to the model. Otherwise, for a simpler model, the noise power at the output of the repeater can be modeled using an additive thermal noise at the input of the amplifier. For an amplifier with noise figure NF, a bandwidth B, and thermal noise with power spectral density N_0, the noise power at the output is then given by $P_{\mathrm{n,X}} = 10 \cdot \log_{10}(N_0 \cdot B) + G_{\mathrm{X}} + \mathrm{NF}$. Measurements at our repeater have shown that noise figure NF increases with decreasing gain G_{X}. Figure 6 shows the results of the noise power measurements.

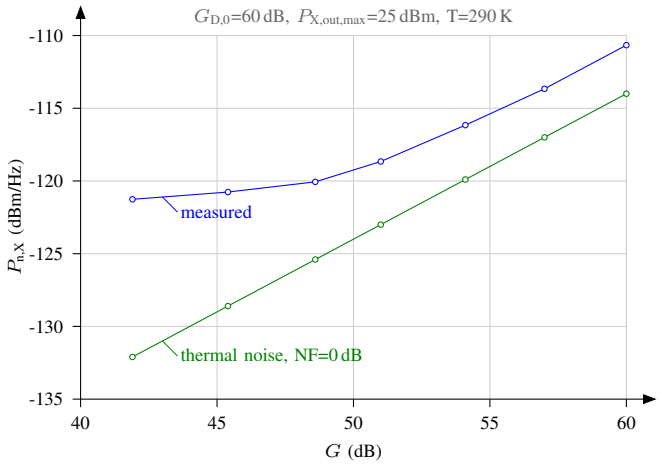

Fig. 6. Noise power density at the output of the repeater.

C. Delay

Depending on the mobile communication system and the actual application of the model, the delay of the repeater needs to be considered. Thereby, when using the full functionality of our repeater, we measure a delay τ of approximately 7.4 µs. The delay can be reduced to values below 3 µs when all features are not being used all at once.

VI. Measurements of the Outdoor Pathloss

To obtain realistic values of the outdoor pathloss L_{outdoor}, we performed a drive test with our train along the main railroad track between the eastern and the western parts of Austria, including a route through Germany. We used a modified NEMO [17] measurement phone, with external antenna connectors connected to the rooftop antennas of the train. During the whole measurement, the phone performed a continuous HTTP download using LTE locked to the 800 MHz band. More details on this drive-test can be found in [18]. Figure 7 shows the measured outdoor pathloss L_{outdoor} split into two sections by the different deployment strategies of the BTSs. The first section was from Wien to Salzburg in Austria, whereas the second section was from Freilassing to Kiefersfelden in Germany. In Austria, there is an optimized trackside deployment of BTSs; in Germany, there is the typical rural deployment focusing on mobile coverage for the resident population. This results in an approximately 20 dB smaller pathloss in Austria.

VII. Discussion of the Setup under Test

Using our model and the corresponding measured parameters, we can estimate the DL pathloss L_{UE} for the UE on

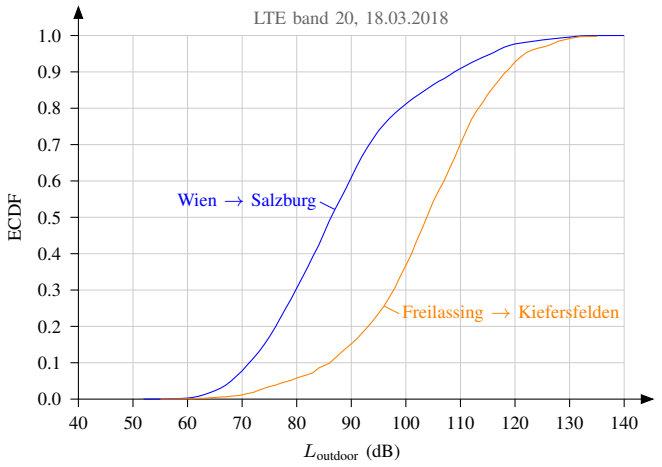

Fig. 7. Measured pathloss for two-coverage scenarios: trackside deployment (blue), rural deployment (orange).

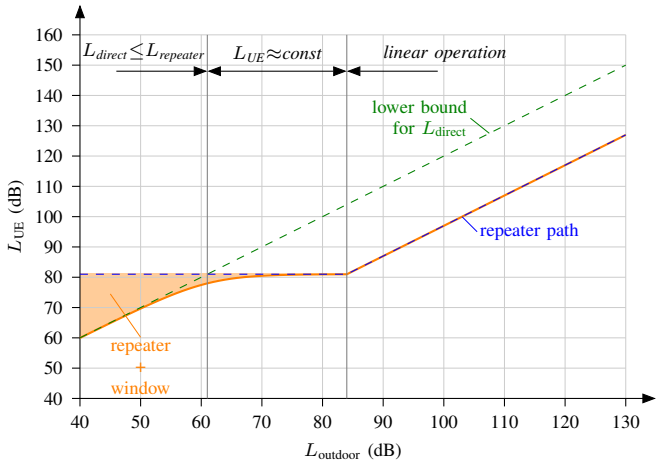

Fig. 8. Pathloss model for the DL path of the ITR deployment under test. The three regions represent the different operation modes of the setup.

board the train being tested. This allows us to define different regions of operation of a train that uses an ITR. Furthermore, the results of the drive-test in Section VI allows us to test the efficiency of an ITR for the scenarios measured.

A. DL Pathloss

For the evaluation of the DL pathloss we consider the following:

- The BTS transmits a fully loaded LTE carrier at 800 MHz with a transmit power P_{BTS} of 46 dBm. Note that the actual transmit power depends on the cell load [19]. Therefore, the cell load needs to be taken into account.
- The repeater has a maximum output power $P_{\text{X,out,max}}$ of 25 dBm and a nominal gain $G_{\text{X,0}}$ of 63 dB. The DL path of the repeater saturates at input powers larger than $P_{\text{X,out,max}} - G_{\text{X,0}}$ =-38 dBm. The corresponding minimum outdoor pathloss L_{outdoor} for the linear operation of the repeater calculates to $P_{\text{BTS}} - P_{\text{X,out,max}} + G_{\text{X,0}}$ =84 dB.
- We define a lower bound for the pathloss of the direct path. Thereby, we assume that the outdoor pathloss L_{outdoor} is always smaller than or equal to the pathloss of the direct path in case of an negligible loss of the train carriage. The lower bound for the pathloss of the direct path is then given by $L_{\text{outdoor}} + L_{\text{window}}$. We consider a window penetration loss of 20 dB.
- We evaluate the DL pathloss for an UE located at measurement location 3. There, the cabin pathloss L_{cabin} is approximately 60 dB.

Figure 8 shows the estimated pathloss from the BTS to the UE as a function of the outdoor pathloss L_{outdoor}. We can split the result into the following three regions of operation:

- *Linear operation*: In outdoor pathlosses larger than 84 dB, the repeater operates in the linear region, and thus the pathloss of the repeater path is proportional to the outdoor pathloss. The pathloss of the direct path is at least 23 dB larger than that of the repeater path, and thus can be neglected. The total pathloss is 3 dB lower than the outdoor pathloss.
- $L_{UE} \approx const$: The repeater saturates at outdoor pathlosses smaller than 84 dB and fixes the pathloss of the repeater path to 81 dB.
- $L_{direct} \leq L_{repeater}$: In outdoor pathlosses smaller than 61 dB, the pathloss of the direct path may be smaller than that of the repeater path.

B. Efficiency of the Repeater

To compare the efficiency of the DL path of the repeater at different sections of a railroad track, we use the results of the drive-test described in Section VI. Therefore, we need to consider that the actual input power of the repeater depends on the outdoor pathloss, the transmit power of the BTS, and the actual cell load. Furthermore, the received power includes interference from other BTSs. In our LTE drive-test, the actual received power, the same power a repeater would consider for its gain control, corresponds to the Received Signal Strength Indicator (RSSI) that the phone reports. Considering a single LTE carrier in the frequency band of interest, the repeater used in our model operates in the linear region at RSSI values below -38 dBm. In the Austrian section of the drive test, the repeater would then have operated in the linear region at approximately 53% of the time and at approximately 93% of the time in the German section of the track. In our setup, the pathloss of the direct path might be less than that of the repeater path for outdoor pathlosses smaller than 61 dB. In this region, the pathloss of the repeater path is independent of the actual input power of the repeater. In the Austrian section measured in our drive-test, the outdoor pathloss is smaller than 61 dB at approximately 0.5% of the time and at approximately 0.1% of the time in the German section. Thus, the ITR is able to provide good service quality inside the cabin in areas of poor outdoor coverage. Even in cases of optimized trackside deployment, the ITR improves the coverage in more than 99 % of the cases.

VIII. Conclusions

We present a holistic model for an ITR setup. It is built from individual blocks, where each of them can be measured independently from one another. The model considers the effects of variable receive signal strength at the pick-up antenna; pathloss due to the in-train distribution system; and limitations due to isolation, gain, and window penetration loss. We parametrize the model for an existing ITR setup and study its efficiency for two extreme cases of deployment strategy: simple rural and optimized track side. The setup increases coverage in both scenarios in more than 99 % of the cases. The parametrized model can serve as an initial simulation model for ITR setups that mobile operators can integrate into their radio-planning process. It further enables train operators to evaluate current and planned ITR setups.

Acknowledgments

This work has been funded by the ITC, TU Wien. The financial support of the Austrian BMWFW and the National Foundation for Research, Technology, and Development is gratefully acknowledged. The research has been cofinanced by the Czech GA CR (Project No. 17-18675S and No. 13-38735S), and by the Czech Ministry of Education in the frame of the National Sustainability Program under grant LO1401, and supported by the Austrian FFG, Bridge Project No. 871261. We thank A1 Telekom Austria AG for their support and Kei Cuevas for the proofreading.

References

[1] P. Lähdekorpi, T. Isotalo, S. U. Khan, and J. Lempiäinen, "Implementation Aspects of RF-repeaters in Cellular Networks," in *21st Annual IEEE International Symposium on Personal, Indoor and Mobile Radio Communications (PIMRC)*, Istanbul, Turkey, Sep. 2010.

[2] M. Madani Fadoul, M. Morsin, C. Y. Leow, and A. Eteng, "Using Amplify-and-forward Relay for Coverage Extension in Indoor Environments," *Journal of Theoretical and Applied Information Technology*, vol. 91, no. 2, pp. 304–312, Sep. 2016.

[3] F. Kaltenberger, A. Byiringiro, G. Arvanitakis, R. Ghaddab, D. Nussbaum, R. Knopp, M. Bernineau, Y. Cocheril, H. Philippe, and E. Simon, "Broadband Wireless Channel Measurements for High Speed Trains," in *IEEE International Conference on Communications (ICC)*, Jun. 2015.

[4] K. Guan, Z. Zhong, B. Ai, and T. Kürner, "Propagation Measurements and Analysis for Train Stations of High-Speed Railway at 930 MHz," *IEEE Transactions on Vehicular Technology*, vol. 63, no. 8, pp. 3499–3516, Oct. 2014.

[5] C. Wang, A. Ghazal, B. Ai, Y. Liu, and P. Fan, "Channel Measurements and Models for High-Speed Train Communication Systems: A Survey," *IEEE Communications Surveys Tutorials*, vol. 18, no. 2, pp. 974–987, Secondquarter 2016.

[6] T. Domínguez-Bolaño, J. Rodríguez-Piñeiro, J. A. García-Naya, and L. Castedo, "Experimental Characterization of LTE Wireless Links in High-Speed Trains," *Wireless Communications and Mobile Computing*, vol. 2017, Sep. 2017.

[7] M. K. Müller, M. Taranetz, and M. Rupp, "Providing Current and Future Cellular Services to High Speed Trains," *IEEE Communications Magazine*, Oct. 2015.

[8] J. Rodríguez-Piñeiro, M. Lerch, J. A. García-Naya, S. Caban, M. Rupp, and L. Castedo, "Emulating Extreme Velocities of Mobile LTE Receivers in the Downlink," *EURASIP Journal on Wireless Communications and Networking*, vol. 2015, no. 1, p. 106, Apr. 2015.

[9] T. Berisha, P. Svoboda, S. Ojak, and C. Mecklenbräuker, "Cellular Network Quality Improvements for High Speed Train Passengers by onboard Amplify-and-Forward Relays," in *13th International Symposium on Wireless Communication Systems*, Poznan, Poland, Sep. 2016.

[10] ——, "SegHyPer: Segmentation- and Hypothesis based Network Performance Evaluation for High Speed Train Users," in *IEEE International Conference on Communications (ICC)*, May 2017.

[11] T. Berisha, P. Svoboda, S. Ojak, and C. Mecklenbrccuker, "Benchmarking In-Train Coverage Measurements of Mobile Cellular Users," in *IEEE 86th Vehicular Technology Conference (VTC2017-Fall)*, Toronto, Canada, Sep. 2017.

[12] M. Tolstrup, *Indoor Radio Planning: A Practical Guide for 2G, 3G and 4G*, 3rd ed. Wiley, Apr. 2015.

[13] M. Lerch, P. Svoboda, S. Ojak, M. Rupp, and C. Mecklenbräuker, "Distributed Measurements of the Penetration Loss of Railroad Cars," in *IEEE 86th Vehicular Technology Conference (VTC2017-Fall)*, Toronto, Canada, Sep. 2017.

[14] M. Rindler, S. Caban, M. Lerch, P. Svoboda, and M. Rupp, "Swift Indoor Benchmarking Methodology for Mobile Broadband Networks," in *IEEE 86th Vehicular Technology Conference (VTC2017-Fall)*, Toronto, Canada, Sep. 2017.

[15] Panorama antennas "Great White" MIMO antenna. (Date last accessed January 19, 2019). [Online]: http://www.panorama-antennas.com/site/index.php?route=product/product&product_id=70

[16] Comlab Multiband Intrain Repeater RUD19-5. (Date last accessed January 15, 2019). [Online]: https://www.comlab.ch/en/products/repeaters/multi_band_repeater.html

[17] Keysight Technologies Nemo Handy Handheld Measurement Solution. (Date last accessed October 10, 2018). [Online]: https://www.keysight.com/en/pd-2767485-pn-NTH00000A/nemo-handy

[18] M. Lerch, P. Svoboda, O. Trindade, J. Resch, V. Raida, and M. Rupp, "Identifying Multipath Propagation in Vehicular Repeater Deployments by LTE Measurements," in *IEEE 89th Vehicular Technology Conference (VTC2019-Spring)*, Kuala Lumpur, Malaysia, 2019.

[19] V. Raida, M. Lerch, P. Svoboda, and M. Rupp, "Deriving Cell Load from RSRQ Measurements," in *2018 Network Traffic Measurement and Analysis Conference (TMA)*, Vienna, Austria, Jun. 2018.